



## Effect of Segmental Joint on Internal Forces in Tunnel Lining under Seismic Loading by Numerical Method

G.H. Ranjbar<sup>1</sup>, K. Shahriar<sup>2\*</sup> and K. Ahangari<sup>1</sup>

*1-Faculty of Mining Engineering, Science and Research Branch, Islamic Azad University, Tehran, Iran*  
*2-Faculty of Mining and Metallurgy Engineering, Amirkabir University of Technology, Tehran, Iran*

Received 1 October 2019; received in revised form 19 April 2020; accepted 23 April 2020

### Keywords

*Segmental Lining*

*Joint Stiffness*

*Seismic Loading*

*Numerical Method*

*Internal Forces*

### Abstract

Although segmental tunnel linings are often used for seismic areas, the influence of segment joints on the segmental lining behavior under seismic loading has not been thoroughly considered in the literature. This paper presents the results of a numerical study investigating the effects of the rotational, axial, and radial joint stiffness of the longitudinal joints on the structural forces in segmental tunnel lining under seismic loading. A 3D finite element method is adapted to establish elaborate numerical models of the segments. The validity of the numerical model was tested by comparing the results obtained with the well-known analytical methods presented by Wang and Penzien. The results demonstrate that by increasing the rotational stiffness of the segmental joint, the bending moment increases. When the rotational stiffness ratio is less than 0.5, the positive and negative bending moment variations are more. The numerical modeling results show the variations in the bending moment and the difference between the positive and negative bending moment values increased by increasing the acceleration of seismic loading. Moreover, it is significant for the values. By increasing the rotational stiffness ratio of the segmental joint, the axial force ratio decreases. By increasing the axial and shear stiffness ratio of segmental joint, the variations in the bending moment and axial force in segmental lining is not significant and is ignorable in designing segmental lining.

### 1. Introduction

The support system of underground facilities in seismic zones must be designed to withstand static overburden loads and accommodate the additional deformations imposed by earthquake-induced motions [1]. Ovaling or racking deformations are the components having the most significant influence on the tunnel lining under seismic loading except for the case of the tunnel being directly sheared by a fault [2]. The ovaling deformations on acircular tunnel are produced by wave propagation perpendicular to tunnel axis [3]. According to the previous studies, propagation of vertical shear wave causing vibration in the horizontal direction is most effective on producing ovaling deformation around the tunnel [4].

The analytical and numerical methods are used to determine the internal forces and displacement of tunnel lining under ovaling deformation. Based on the closed form solutions recommended by Wang (1993), the proposed analytical equations have been modified in terms of axial force, bending moments, and displacements under the external loading conditions [4].

Penzien and Wu have developed similar analytical solutions for thrust, shear, and moment in the tunnel lining due to racking deformation [5]. Later, Penzien provided a complementary analytical procedure to evaluate the racking deformation of rectangular and circular tunnels [6]. Hashash (2001, 2005), by comparing these two methods, has revealed that the calculated

forces and displacements are identical for the full-slip assumption; however, the Penzien's solution has resulted in a much lower estimation of maximum thrusts compared to the Wang's solution for the no-slip assumption [7, 8]. Park has also reported this difference [9]. Generally, the closed-form solutions are limited to the following assumptions:

- The homogenous soil mass and the tunnel lining are assumed to be linear elastic and massless materials;
- Tunnel is circular with uniform thickness and without the joints;
- The effect of construction sequence is not considered [10].

In order to overcome the deficiencies of the analytical methods, the recent common trend is to use the 2D numerical analysis techniques (e.g. [2, 11]) or 3D numerical analyses (e.g. [12, 13, 16]). Segmental tunnel linings are often used for seismic areas in many countries such as the United States, Japan, Venezuela, Puerto Rico, Iran, Taiwan, Turkey, Spain, Italy, and Greece. Owing to the high flexibility achieved through the joints between segments, segmental linings can accommodate deformations with little or no damage; therefore, their performance is better than a continuous lining during an earthquake. The presence of segment joints in the tunnel lining reduces the stresses and strains in the lining [11].

The effects of joints on the internal forces and displacements should be considered in the lining design [14]. Recently, the behavior of segmental joints in concrete precast tunnel lining has been one of the interesting topics. The radial (or longitudinal) joints are the connection parts between the segments in the lining ring as well as the circumferential joints linking different rings. The stiffness of the longitudinal and circumferential joints is important to evaluate the geotechnical actions on the lining [15].

In the literature, the effects of segmental joints on the tunnel lining are usually considered in both the direct and indirect methods. In the indirect methods, the tunnel lining is perceived as a rigid lining ring embedded on a continuous ground model to consider the segmental lining as a continuous ring with a reduced rigidity by applying a reduction factor,  $\eta$ , to the bending stiffness (EI) of the tunnel lining [16]:

$$\eta = \frac{(EI)_{eq}}{EI} \quad (1)$$

where  $(EI)_{eq}$  is the bending stiffness of the tunnel segmental lining and (EI) is the bending stiffness of the continuous lining.

Wood has suggested that the segmental joint behaves like a set of partial hinges in the lining structure. Therefore, the effective moment of inertia of the overall lining,  $I_e$ , should be reduced to consider the joint characteristics, which are written as follow [17]:

$$I_e = I_j + \left(\frac{4}{n}\right)^2 I \quad , \quad (I_e \leq I, n)4 \quad (2)$$

where I and  $I_j$  are the moments of inertia of the intact liner and segmental joint, respectively, and n is the number of joints in the liner.

The Japanese Society of Civil Engineers (JSCE) descriptively recommends reducing the rigidity of the continuous liner structure by 20-40%. Nevertheless, most of the Japanese tunneling projects require a full scale prototype test to verify the bending moment reduction factor [18].

Liu and Hou have proposed an analytical correlation for the moment reduction factor based on the maximum horizontal displacement of a continuous ring:

$$\eta = \frac{1}{1 + b} \quad (3)$$

where:

$$b = \frac{3EI}{RK_{RO}} \sum_{i=1}^m \cos\varphi_i \cos 2\varphi_i \quad (0 < \varphi_i < \frac{\pi}{2}) \quad (4)$$

where EI is the bending rigidity of the tunnel lining per length,  $K_{RO}$  is the rotational spring stiffness of the joints defined as the bending moment per length required to develop a rotation angle along a joint of assembled segments,  $\varphi_i$  is the angle measured from the vertical direction around the tunnel of the  $i^{th}$  joint in the range of 0-90°, m is the number of joints in the range of 0-90°, and R is the tunnel calculated radius [19].

Through analytical analysis, Lee and Ge have provided graphical relationships between the effective segmental lining stiffness, reduction factor of the bending rigidity ( $\eta$ ), and soil resistance (Ks). In order to illustrate the relationship between the reduction factor of the bending rigidity ( $\eta$ ) and the joint stiffness, a dimensionless parameter called the joint stiffness ratio,  $\lambda = K_\theta l / EI$ , has been introduced to represent the relative stiffness of the joint over the rigidity of the lining segment. The calculation length, l, is usually considered 1 m to represent the typical unit length of a lining segment.  $K_\theta$  is the flexural (rotational) stiffness of the joint (per

unit length), which is assumed to be a constant [20].

Blom has introduced a reduction factor formula that can be applied to the flexural rigidity of a full continuous ring to consider the global influence of the joint:

$$\eta = \frac{1}{1 + \frac{3t^3}{4l_t^2 r} (C_X^* + C_Y^*)} \quad (5)$$

where:

$$C_X^* = \sum_{-\frac{\pi}{2}(\beta_i)}^{\beta_i(\frac{\pi}{2})} \cos(\beta_i) \cos(2\beta_i) \quad (6)$$

$$C_Y^* = - \sum_{0(\beta_i)}^{\beta_i(\pi)} \sin(\beta_i) \cos(2\beta_i)$$

where  $\beta_i$  is the angle at the  $i^{th}$  joint location, measured from the tunnel crown. A diagram presenting the reduction factor  $\eta$  of the bending stiffness as a function of the contact area in the longitudinal joint ( $l_t$ ), segmental thickness ( $t$ ), and radius ( $R$ ) for several numbers of segments of a single ring has also been introduced based on this formula [21].

These methods have some drawbacks that are required to be regarded, as follow:

- The effect of joint location on the internal forces induced in the tunnel lining is not shown;
- The dependency of the lining behavior on the change of characteristics like the rotation stiffness  $K_\theta$  between joints in a ring is not possible to be considered.

Owing to the mentioned reasons, it is more precise to use the designed methods in which the presence of joints in the lining is considered directly. In the direct methods, segmental joints are directly added to the tunnel lining.

Blom has proposed an analytical method considering both the interaction between successive rings composed of the elastic jointed segments and the soil-structure interaction. In this method, the soil is modelled through a bed of constant radial spring around the lining. The author considers two sets of elastic blocks: each set forms a circular ring [22].

Naggar and Hinchberger have introduced an analytical solution for jointed tunnel lining that can be idealized as an inner jointed segmental lining and an outer thick-walled cylinder embedded in homogenous infinite elastic soil and rock. One of the main disadvantages of the Naggar and Hinchberger's method is the

symmetrical distribution of the joints regarding the vertical axis of the tunnel cross-section [23].

The rapid progress in the development of computer codes and the limitation of analytical methods have led to an increase in the use of numerical methods to design the tunnel lining.

In numerical analysis, two main techniques are applied to model the ground-structure interaction. The first technique involves the use of discrete springs, and is based on the Winkler's theory, focusing on the structural behavior of the segmental lining [21]. The second approach uses the full ground model using finite elements [24, 25]. Although heavy computational efforts are required, the second approach generally provides more accurate results.

Hefny et al. have numerically studied the influence of the joint number, joint orientation, lateral earth pressure factor, and tunnel depth on the bending moment induced in a 6-m diameter segmental tunnel lining using a finite element analysis program. In their analysis, the segmental joints were assumed to be fully hinged (the joint capacity of the transmitting partial moment by the joints was not considered). The results obtained indicated that increasing the joint number reduced the maximum bending moment induced in the lining. The maximum bending moment induced in the lining becomes negligibly small when the joint number exceeds 8 [26].

Blom et al. have proposed a detailed 3D FEM analysis of the tunnel structures using the Ansys FEM software. This model allows the effects of the ground reaction, interaction between segments, packing material between rings, jacking forces, grout phase changes from a liquid state to a solid state, and assembly segments in a ring to be taken into account. The interaction between the segments (in all directions) was realized by applying the contact elements [21].

This paper presents the results of a numerical study investigating the effect of the rotational joint stiffness of the longitudinal joints on the structural forces in segmental tunnel lining under seismic loading. A 3D finite element method was adapted to develop elaborate numerical models of segments. The validity of the numerical model was tested by comparing the results obtained with the well-known analytical methods presented by Wang and Penzin.

## 2. Mashhad subway tunnel (line 2)

For the numerical modeling in this work, the geotechnical parameters of the Mashhad subway tunnel (line 2) were used as the input data to

analyze the results. The length of this line is proximately 14.3 km with 12 stations. The soil of the tunnel route mainly includes layers of fine clay and coarse sand. The underground water height differs only under the roof of the tunnel, and the tunnel depth differs from 13.5 m to 21.65 m along the route. Line 2 of the Mashhad subway tunnel is mechanically excavated by TBM. Two TBMs, one from the northern shaft and the other

from the southern shaft, excavate the tunnel. The tunnel support lining is a precast type of segments with 35 cm thickness and 1.5 m width assembled at the back of TBM; in one ring of the tunnel lining, seven segments and one key segment are used. Table 1 shows the mechanical parameters of the soil layer and segments used in numerical modeling [27].

**Table 1. Mechanical parameters of the soil layer and segments [27].**

Parameter	Elasticity module (MPa)	Poisson ratio	Specific weight (kg/m <sup>3</sup> )
Segment	35000	0.2	2500
Soil	30	0.3	1650

**3. Numerical modeling of tunnel under seismic loading**

Figure 1 shows the 3D numerical model used in the present work using the finite element program ABAQUS. It was assumed that the behavior of the tunnel structure and the soil mass was linearly elastic. The whole tunnel was simulated due to the arbitrary distribution of the joints along the tunnel wall boundary. The numerical model was 160 m wide in the y-direction, 37 m high in the z-direction, and 4.5 m deep in the x-direction, and consisted of approximately 105480 zones and 115522 grid points. In this work, a time history analysis was conducted using  $u = u_{max} \sin(\omega t)$  at the bottom boundary of the numerical model for three peak acceleration levels ( $a_{max} = 0.1g, 0.2g$  and  $0.3g$ ), where  $u$  is the horizontal displacement

at time  $t$ ,  $u_{max}$  is the maximum horizontal displacement, and  $\omega$  is the angular frequency. The soil volume was discretized into 3D solid continuum 8-node linear brick elements (C3D8R) having 3 freedom degrees for nodes and was suitable for the surrounding soil of the tunnel and 3D solid continuum 8-node linear infinite elements (CIN3D8) in the right and left boundaries of the model to provide quiet boundaries to the finite element model in a dynamic analysis. The tunnel segments were modeled using the embedded shell elements due to its thin thickness compared with the tunnel diagonal. 4-node linear shell elements (S4R) were used having 6 freedom degrees for nodes (Figure 2) [28].

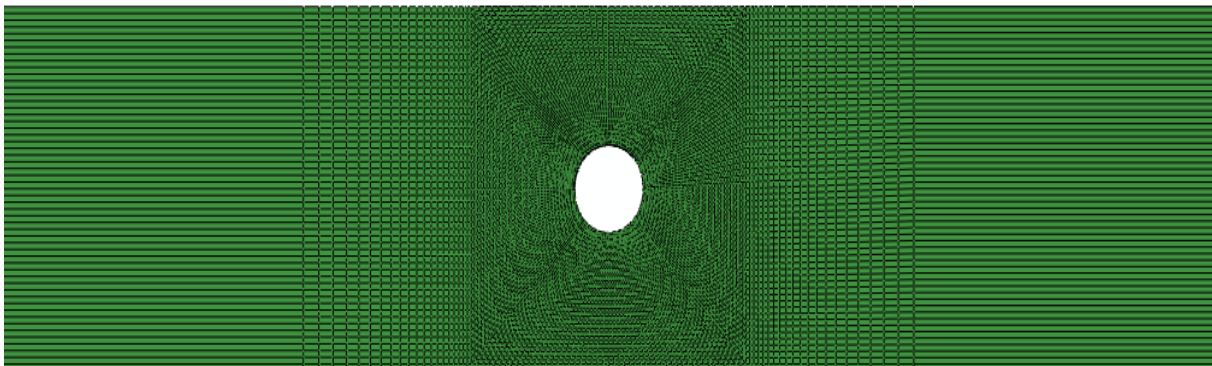


**Figure 1. 3D numerical model of the surrounding soil.**

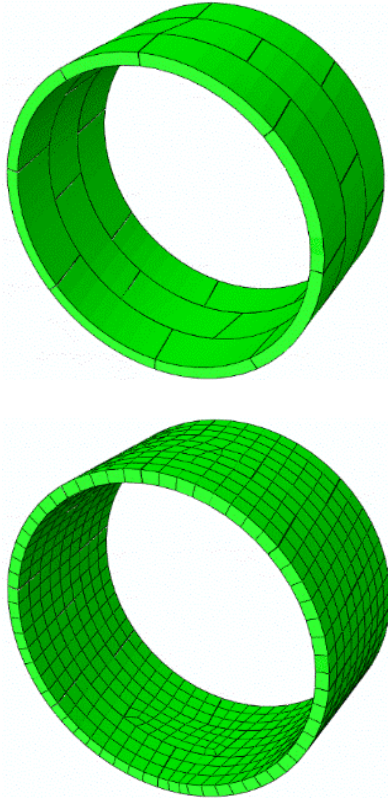


Figure 2. 3D numerical model of the segments.

In the structural analysis, the segmental joint can be considered as an elastic pin, and its stiffness characteristics can be simulated by rotational or revolving stiffness ( $K_R$ ), axial or normal stiffness ( $K_A$ ), and shear stiffness ( $K_S$ ) (Figure 3). The value for  $K_R$  is defined as the bending moment-per-unit length required to make the unit revolving angle along with the segment mounted joints. Similarly, the axial stiffness ( $K_A$ ) and the radial stiffness ( $K_S$ ) are defined as the axial force and shear force of the length unit, respectively, which are required to make the unit axial and radial movements in the assumed joint [11].

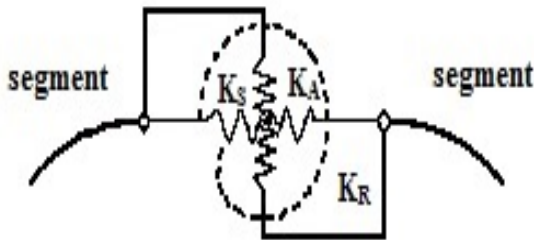


Figure 3. Shear ( $K_S$ ), axial ( $K_A$ ), and rotational stiffness ( $K_R$ ) of the joint [11].

In the numerical model, the segmental joints are simulated using the connector elements between the shell elements. The connector element functions as a link between two shell elements in which the segments are allowed to move toward each other. The dimensionless parameters of the rotational joint stiffness ratio ( $\lambda_R = K_R l / EI$ ), the axial joint stiffness ratio ( $\lambda_A = K_A l / EA$ ), and the shear joint stiffness ratio ( $\lambda_S = K_S l / GA$ ), which were introduced by Lee (2001) [20], were used to simulate the linear elastic behavior of the segmental joints (Figure 4).

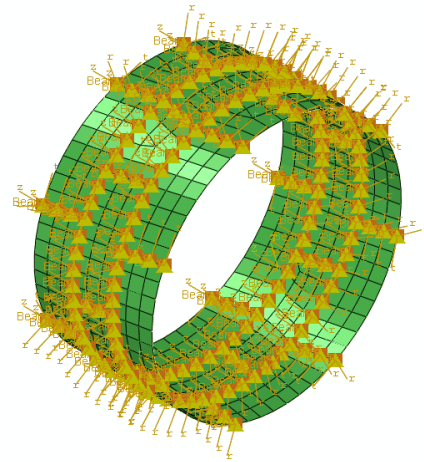


Figure 4. The connector elements between shell elements and the cylindrical coordinate system for applying the rotational, radial, and axial stiffness.

According to the previous studies, the main variation in the segmental lining forces, moment, and displacement belonging to the joint stiffness ratio is between zero and one. Therefore, the values of 0.1, 0.2, 0.3, 0.5, 0.8, and 1 were considered the values of the segmental joint stiffness ratio in the analyses. For simplicity, the rotational, axial, and shear stiffness of all joints was considered in one similar ring. The embedded shell elements were attached to the brick element faces along the tunnel perimeter with no-slip condition.

#### 4. Validation of numerical model

Numerical simulations of the circular tunnel were conducted and compared to the well-known closed-form solution of Wang and Penzien according to the suggestion made by Hashash *et al.* to validate the numerical model for further studies. Figures 5 and 6 show the graphs for the internal moments and axial forces appearing on the tunnel lining based on the analytical methods

proposed by Wang, Penzien, and Wu, and the numerical method for continuous and segmental lining, respectively. The figures help to compare the results of different methods including the Wang's analytical method, Penzien and Wu's analytical method, and 3D numerical method using the ABAQUS program. In the case of  $\lambda = 1$  for the segmental joints, the bending moments were quite close to each other, and the deviation was not large (Figure 5). The internal forces

obtained on the segmental tunnel lining are not significantly different from the results of the Wang's method. However, the value of the axial force obtained from the Wang's method and the numerical method is much higher than the value given by Penzien (Figure 6). Power *et al.* (1996) have also noted this observation. Figure 7 shows the bending moment and axial force obtained by the numerical method for segmental lining ( $\lambda = 1$ ) and continuous lining.

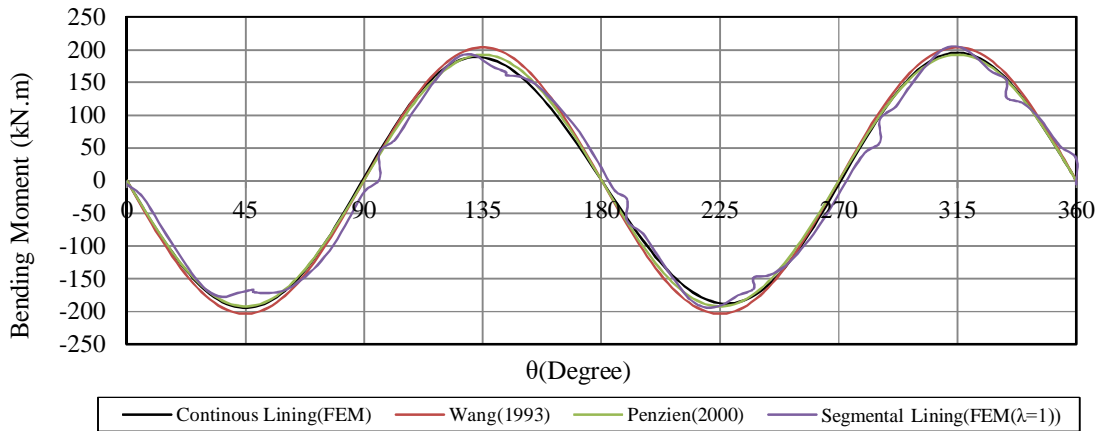


Figure 5. Comparisons of the bending moment obtained by different methods (analytical and numerical).

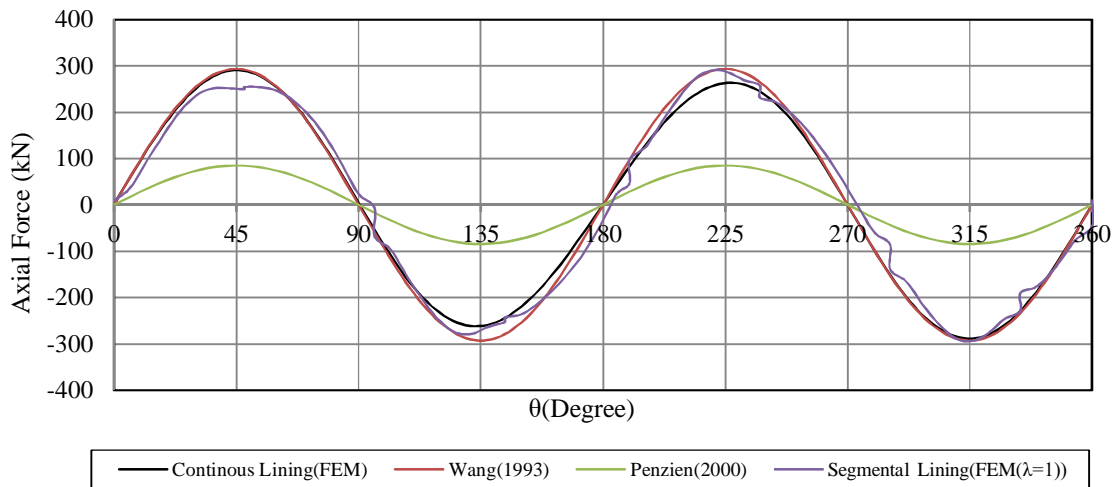


Figure 6. Comparisons of the axial force obtained by different methods (analytical and numerical).

## 5. Effect of segmental joint stiffness on internal forces of tunnel lining

### 5.1. Effect of rotation stiffness

The numerical modeling results showed that the variations in the bending moment and difference between positive and negative bending moment values increased with increase in the acceleration of seismic loading. Moreover, it is significant for the  $\lambda \leq 0.5$  values. The variations in the positive and negative bending moments are approximately

similar (Figure 8). Although the axial force variation is less than the bending moment, it increases for a higher acceleration like a bending moment variation (Figure 9). As shown in Figure 10, by reducing the rotational stiffness, the axial force increases slightly, and the bending moment decreases; therefore, it can be concluded that the bearing capacity of the segmental lining increases with decrease in the rotational stiffness of the segmental joints.

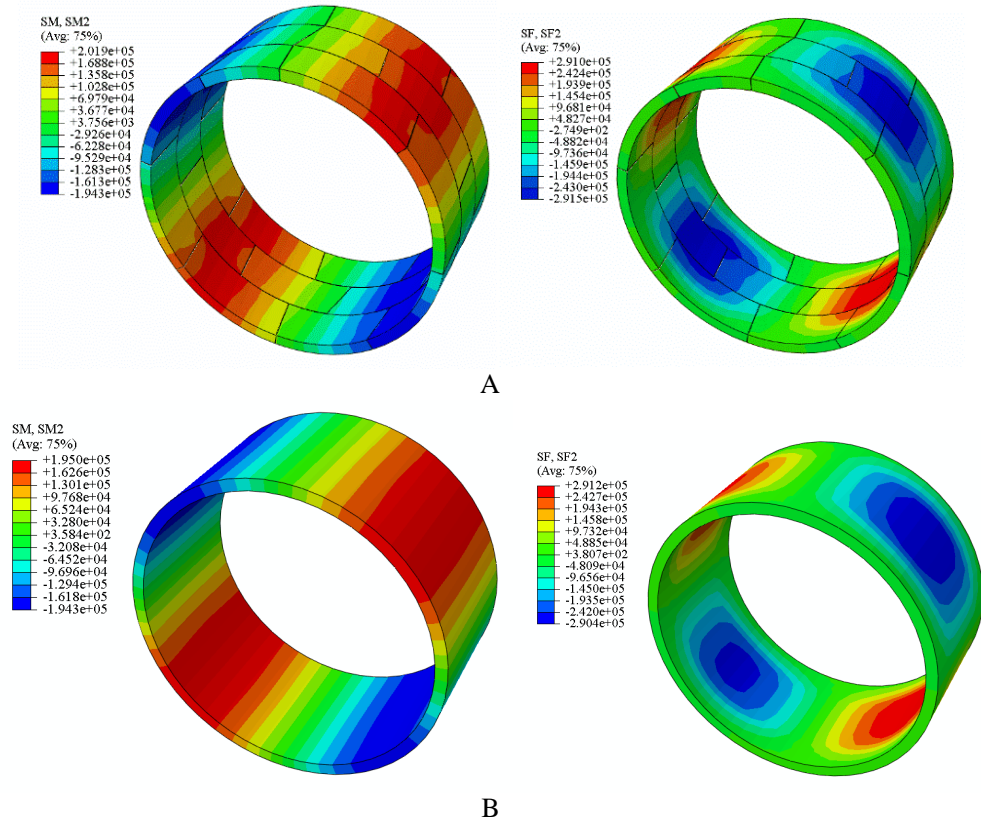


Figure 7. The bending moment and axial force obtained by the numerical method for segmental lining (A) and continuous lining (B).

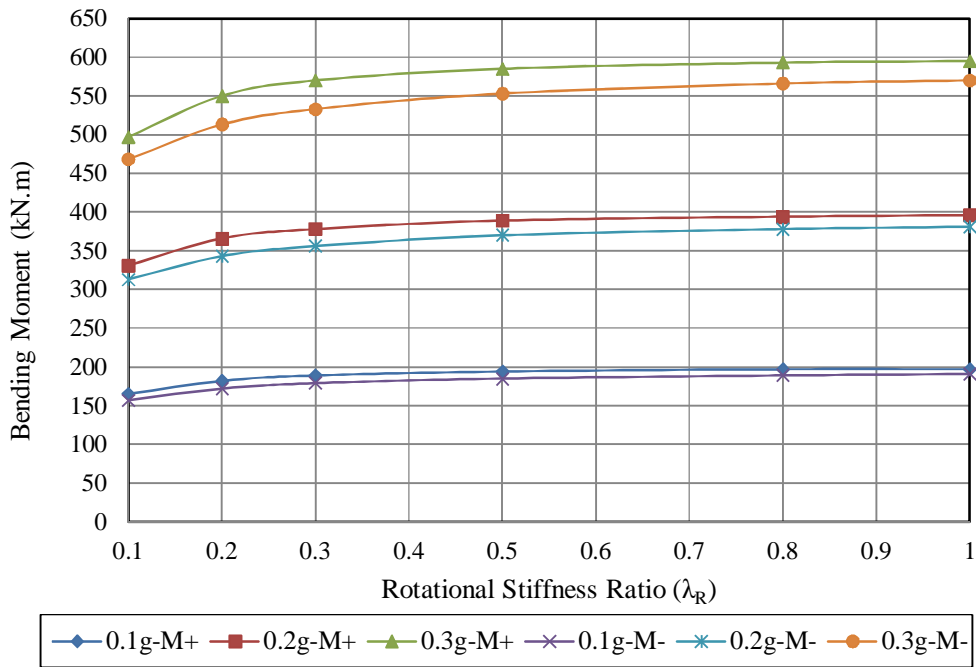


Figure 8. Bending moment variation under the influence of the rotational stiffness of segmental joint.

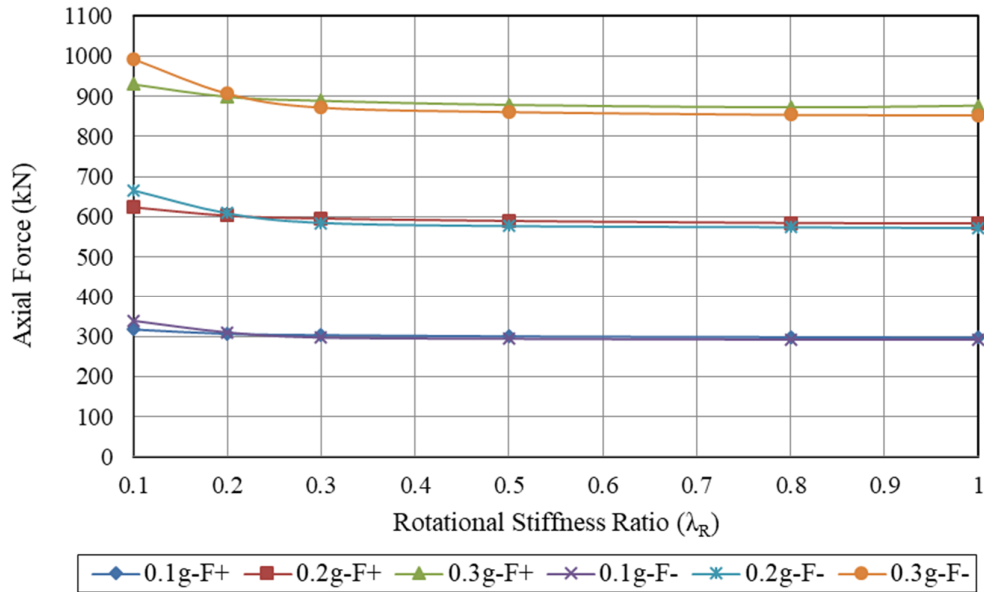


Figure 9. Axial force variation under the influence of the rotational stiffness of segmental joint.

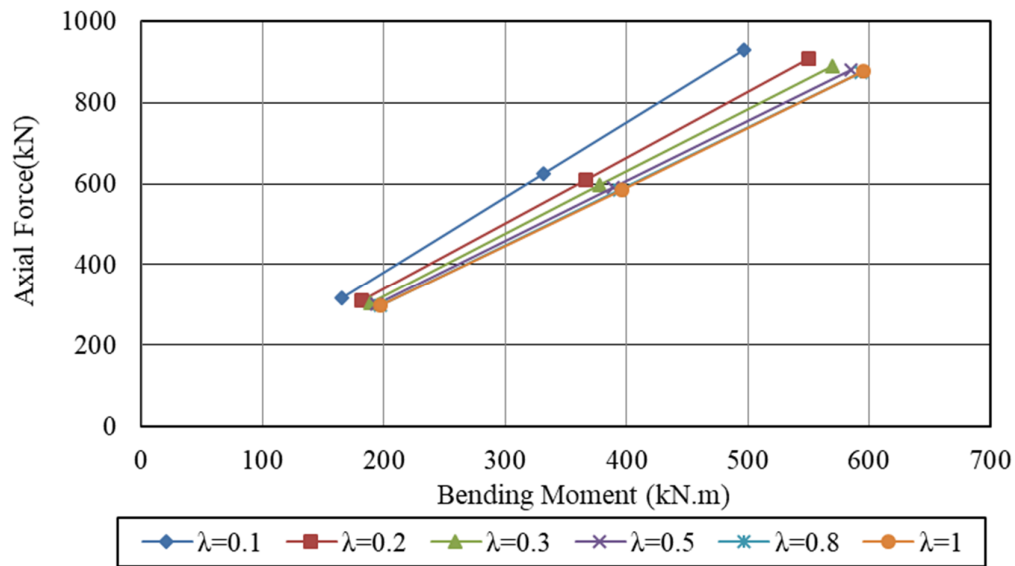


Figure 10. Axial force vs. bending moment under three acceleration levels (0.1g, 0.2g, 0.3g) for six rotational stiffness ratios.

The dimensionless parameters of the bending moment ratio ( $R_M$ ) are defined as the relation of the maximum bending moment of segmental lining with the maximum bending moment for  $\lambda = 1$ , and the axial force ratio ( $R_N$ ) is defined as the relation of the maximum axial force of segmental lining with maximum axial force for  $\lambda = 1$ . These ratios were used in this work to draw charts to analyze the effects of segmental joint stiffness on the lining internal forces. After applying the joint rotational stiffness ratio ( $\lambda_R$ ) for various values in the model and performing

the model for three roof acceleration levels (0.1g, 0.2g, and 0.3g), the figures of the model output data were drawn. As shown in Figure 11, by increasing the rotational stiffness ratio of the segmental joint, the bending moment in segmental lining increases. When the joint rotational stiffness ratio is less than 0.5, the bending moment variation is more significant. The positive and negative bending moment variations in the tunnel lining are similar. As shown in Figure 12, by increasing the rotational stiffness ratio of the segmental joint, the axial force ratio decreases for the positive and negative axial forces. The

variation in the negative axial force is higher than the positive axial force for lower rotational stiffness ratios. However, the variation is not significant. As shown in Figure 13, by decreasing the rotational stiffness ratio of the segmental joint, the rotation in segmental lining increases, whose

variation in rotation decreases for higher stiffness ratios. Figure 14 shows the rotation of segmental lining versus its position from the tunnel crown in a counter-clockwise direction for three peak acceleration levels and  $\lambda_R = 0.1$ .

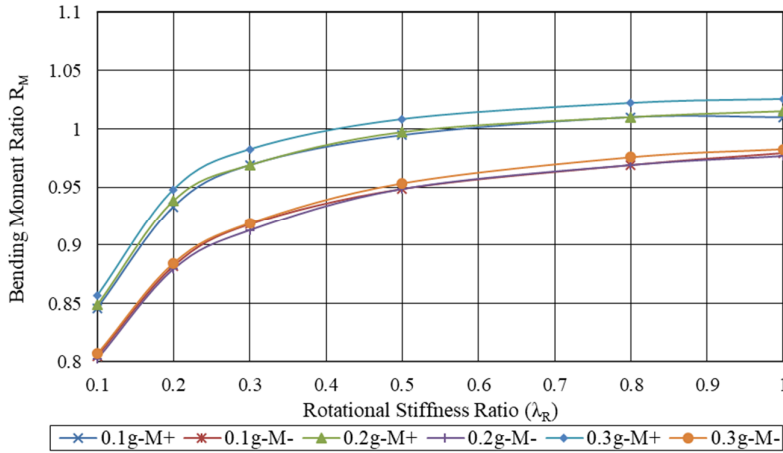


Figure 11. Bending moment ratio vs. rotational joint stiffness ratio for positive and negative bending moments.

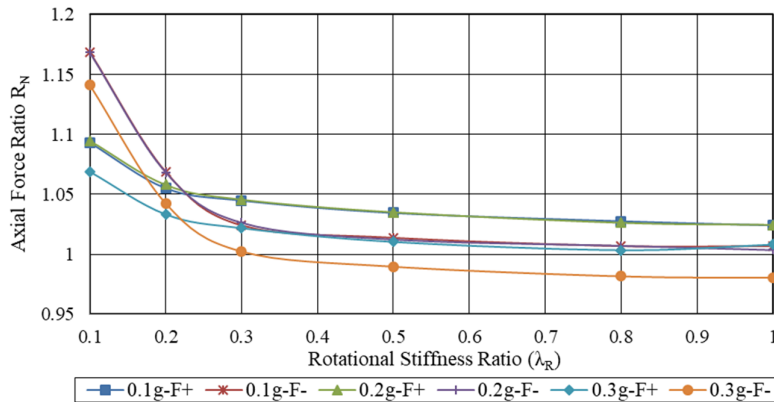


Figure 12. Axial force ratio vs. rotational joint stiffness ratio for positive and negative axial forces.

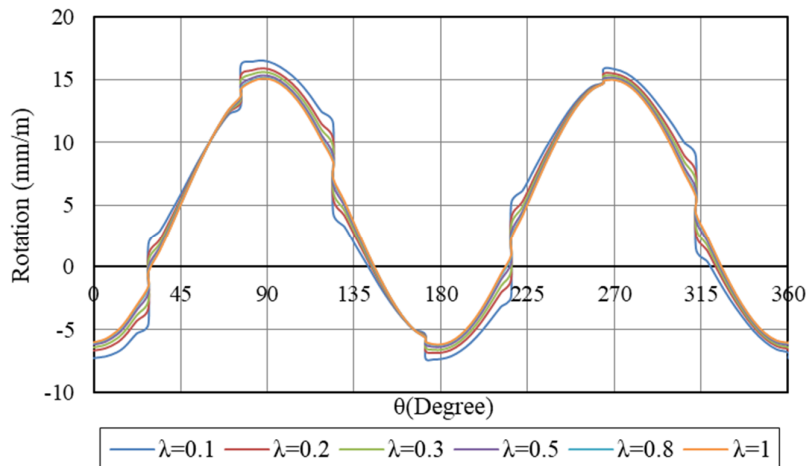
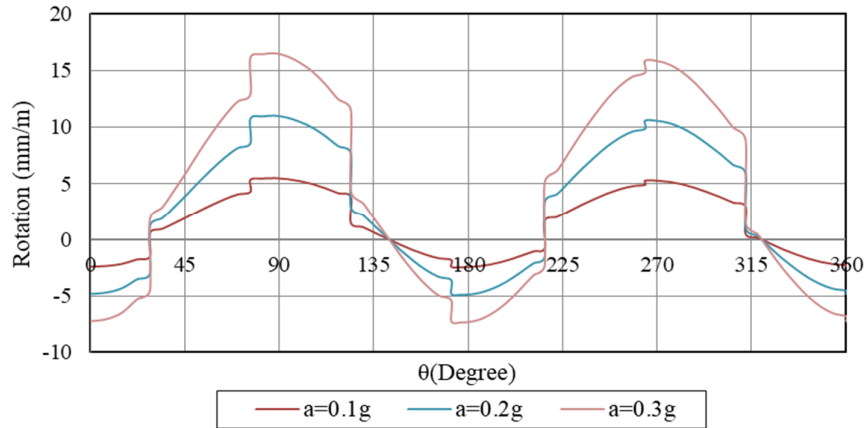


Figure 13. Rotation of segmental lining vs. its position from the tunnel crown in a counter-clockwise direction for different rotational stiffness ratios ( $a = 0.3g$ ).



**Figure 14. Rotation of segmental lining vs. its position from the tunnel crown in a counter-clockwise direction for three roof acceleration levels ( $\lambda_R = 0.1$ ).**

The effect of rotational stiffness on the radial and axial displacements is not significant. However, it

is more effective for lower values of rotational stiffness (Figures 15, 16, 17, 18).

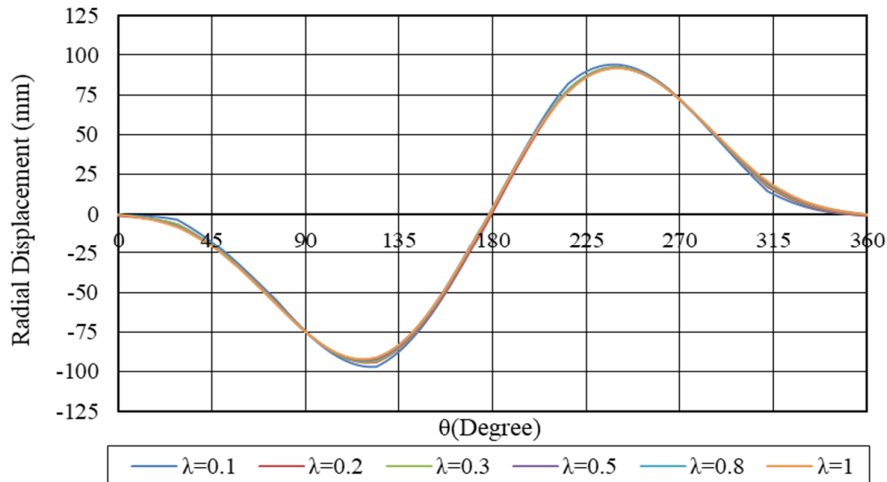


**Figure 15. Radial displacement of segmental lining vs. its position from the tunnel crown in a counter-clockwise direction for different rotational stiffness ratios ( $a = 0.3g$ ).**

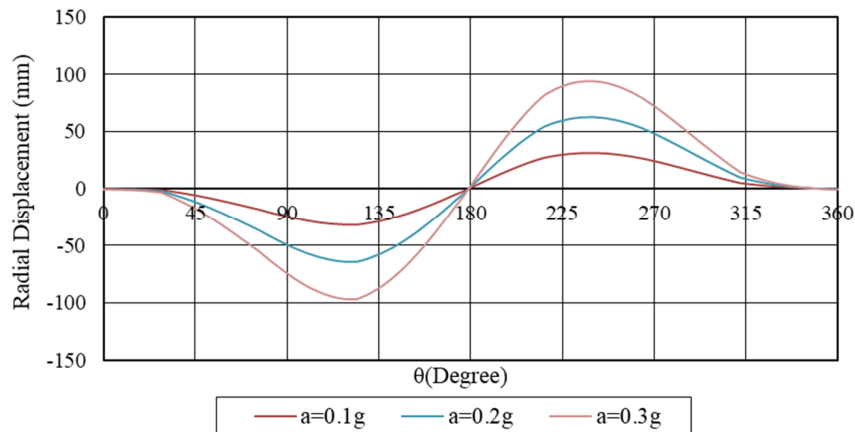


**Figure 16. Radial displacement of segmental lining vs. its position from the tunnel crown in a counter-clockwise direction for three roof acceleration levels ( $\lambda_R = 0.1$ ).**

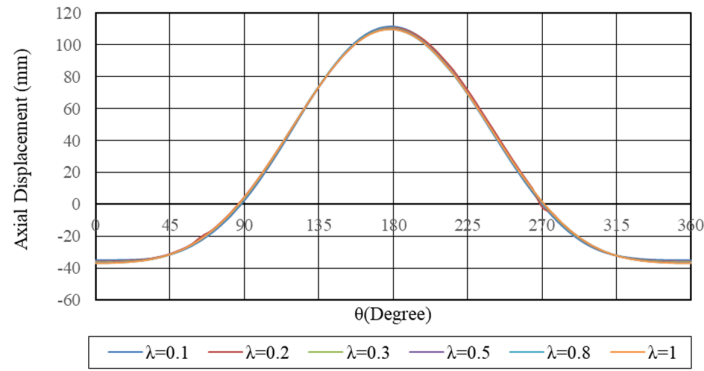


Figure 17. Axial displacement of segmental lining vs. its position from the tunnel crown in a counter-clockwise direction for different rotational stiffness ratios ( $a = 0.3g$ ).

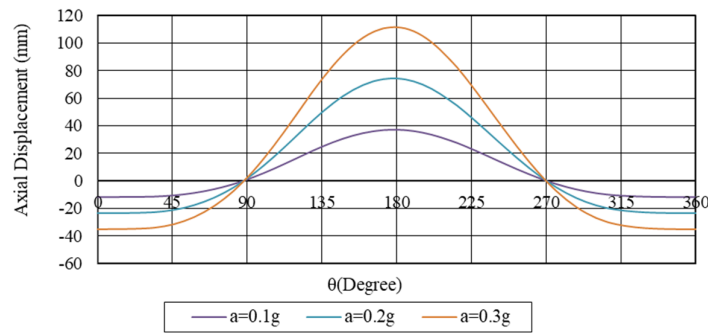


Figure 18. Axial displacement of segmental lining vs. its position from the tunnel crown in a counter-clockwise direction for three roof acceleration levels ( $\lambda_R = 0.1$ ).

### 5.2. Effect of axial stiffness

After applying the joint axial stiffness ratio ( $\lambda_A$ ) for different values in the model and performing the model, the figures of the model output data were drawn. As shown in Figure 19, by increasing the axial stiffness of the segmental joint, the variation in the axial force in segmental lining is ignorable. By increasing the joint axial stiffness ratio, the positive axial force ratio decreases and the negative axial force ratio increases, being

more significant for the lower axial stiffness ratio. According to Figure 20, by increasing the axial stiffness ratio of the segmental joint, the negative bending moment decreases and the positive bending moment increases, and the variation in these values, similar to axial forces, is significant for the lower axial stiffness ratio. However, the variation in the bending moment versus axial force is more significant.

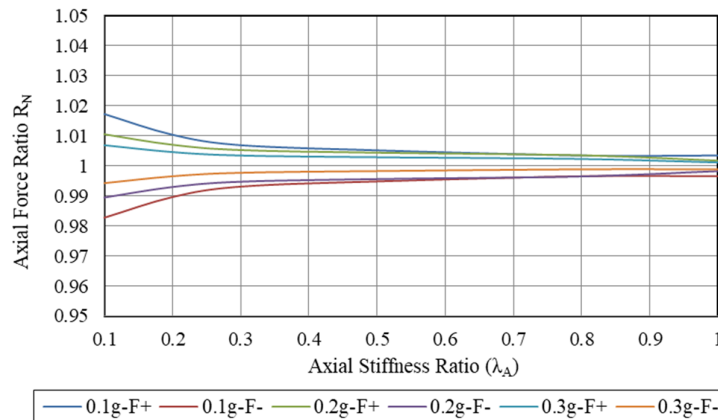


Figure 19. Axial force ratio vs. axial stiffness ratio for positive and negative axial forces.

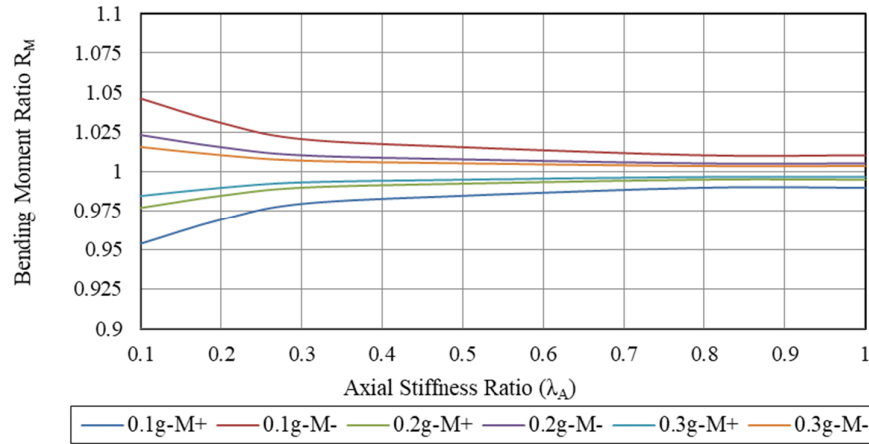


Figure 20. Bending moment ratio vs. axial stiffness ratio for positive and negative bending moments.

### 5.3. Effect of shear stiffness

After applying the joint shear stiffness ratio ( $\lambda_s$ ) for different values in the model and performing the model, the figures of the model output data were drawn. As shown in Figures 21 and 22, by

increasing the shear stiffness ratio of the segmental joint, the variation in the bending moment and axial force in the segmental lining is ignorable.

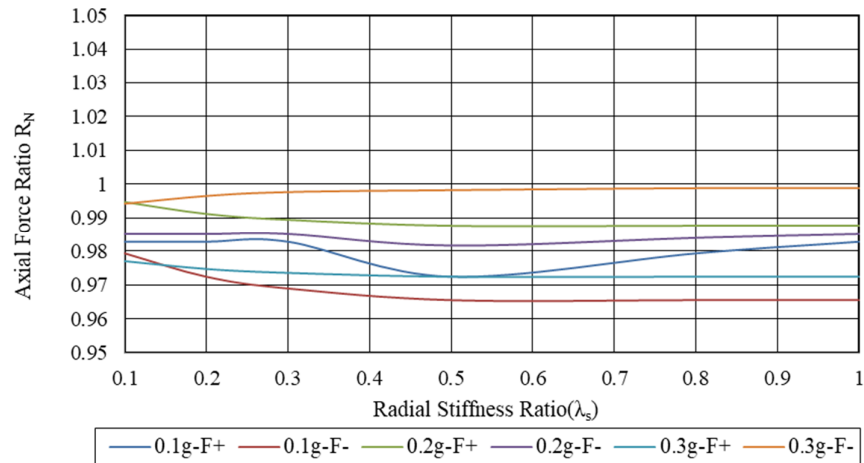


Figure 21. Axial force ratio vs. radial stiffness ratio for positive and negative axial forces.

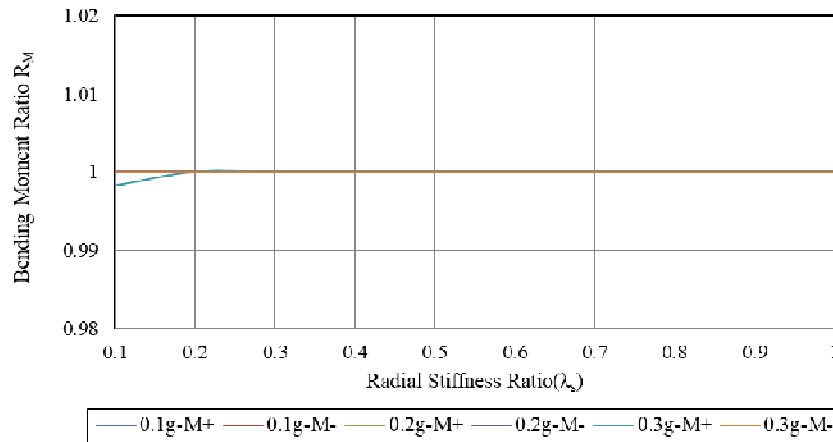


Figure 22. Bending moment ratio vs. radial stiffness ratio for positive and negative bending moments.

## 6. Conclusions

The results of the present work can be divided into three parts, as follows:

### 1- Effect of rotation stiffness

- The variation in the bending moment and difference between positive and negative bending moment values increase for a higher acceleration of seismic loading.
- Although the axial force variation is less than the bending moment, it increases for a higher acceleration like bending moment variation.
- By reducing the rotational stiffness, the axial force increases slightly, and the bending moment decreases; therefore, it can be concluded that the bearing capacity of the segmental lining increases with decrease in the rotational stiffness of segmental joints.
- By decreasing the rotational stiffness ratio of the segmental joint, the rotation in the segmental lining increases, whose variation in rotation decreases for higher stiffness ratios.
- The effect of rotational stiffness on radial and axial displacements is not significant. Nevertheless, it is more effective for lower values of rotational stiffness.

### 2- Effect of axial stiffness

- By increasing the axial stiffness of the segmental joint, the variation in the axial force in the segmental lining is very partial and can be ignored.
- By increasing the joint axial stiffness ratio, the positive axial force ratio decreases and the negative axial force ratio increase, being more significant for the lower axial stiffness ratio.
- By increasing the axial stiffness ratio of the segmental joint, the negative bending moment decreases, the positive bending moment increases, and the variation in these values similar to axial force is significant for the lower axial stiffness ratio. However, the variation in the bending moment against the axial force is more significant.

### 3- Effect of shear stiffness

- By increasing the shear stiffness ratio of the segmental joint, the variation in the bending moment and axial force in the segmental lining is ignorable.

## References

- [1]. Bobet, A. (2003). Effect of pore water pressure on tunnel support during static and seismic loading. *Tunnelling and Underground Space Technology*. 18: 377–393
- [2]. Gomes, R.C., Gouveia, F., Torcato, D. and Santos, J. (2015). Seismic response of shallow circular tunnels in two-layered ground. *Soil Dynamics and Earthquake Engineering*. 75: 37–43
- [3]. Mohammad, C., Pakbaz, A. and Akbar, Yareevand. (2005). 2-D analysis of circular tunnel against earthquake loading. *Tunnelling and Underground Space Technology*. 20: 411–417
- [4]. Wang, J.N. (1993). *Seismic design of tunnels: A state of the art approach*. Parsons Brinkerhoff Quad & Douglas Inc. New York. Monograph 7.
- [5]. Penzien, J. and Ching, L.W. (1998). Stresses in linings of bored tunnels. *Journal of Earthquake Engineering and Structural Dynamics*. 27: 283-300.
- [6]. Penzien, J. (2000). Seismically induced racking of tunnel linings. *Journal of Earthquake Engineering and Structural Dynamics*. 29: 683–691.
- [7]. Hashash, Y.M.A., Hook, J., Schmidt, B. and Yao, J.I. (2001). Seismic design and analysis of underground structure. *Journal of Tunnelling and Underground Space Technology*. 16: 247–293.
- [8]. Hashash, Y.M.A., Park, D. and Yao, J.I. (2005). Ovaling deformations of circular tunnels under seismic loading: an update on seismic design and analysis of underground structures. *Journal of Tunnelling and Underground Space Technology*. 20: 435-441.
- [9] Park, K., Tantayopin, K. and Tontavanich B. (2006). Analytical solutions for seismic design of tunnel lining in Bangkok MRT subway. *Proceedings of the International Symposium on Underground Excavation and Tunneling*. Bangkok, Thailand. 541-550.
- [10]. Sederat, H., Kozak, A., Hashash, Y.M.A., Shamsabadi. A. and Krimotat. A. (2009). Contact interface in seismic analysis of circular tunnels. *Journal of Tunnelling and Underground Space Technology*. 24: 482–90.
- [11]. Do, N.A., Dias, D., Oreste, P. and Djeran-Maigre, I. (2015). 2D numerical investigation of segmental tunnel lining under seismic loading. *Soil Dynamics and Earthquake Engineering*. 72: 66–76.
- [12]. Kramer, G.J., Sederat, H., Kozak, A., Liu, A. and Chai, J. (2007). Seismic response of precast tunnel lining. *Proceedings of the rapid excavation and tunneling conference*. 1225–1242.
- [13] Sliteen, L., Mroueh, H. and Sadek, M. (2013). Three-dimensional modeling of the behaviour of shallow tunnel under seismic load. *20th Congress Rock Mechanics*, France.

- [14]. Nikkhah, M., Mousavi, S.S., Zare, Sh. and Khademhosseini, O. (2017). Evaluation of structural analysis of tunnel segmental lining using beam-spring method and force-method (Case study: Chamshir water conveyance tunnel). *Journal of Mining & Environment*. Vol.8, No.1, 111-130.
- [15]. Caratellia, A., Medaa, A., Rinaldia, Z., Giuliani-Leonardib, S. and Renaultb, F. (2018). On the behavior of radial joints in segmental tunnel linings. *Tunnelling and Underground Space Technology*. 71: 180–192
- [16]. DO, N.A. (2014). Numerical analysis of segmental tunnel lining under static and dynamic loads. Ph.D thesis. Civil Engineering. University of Lyon. France.
- [17]. Wood, A.M.M. (1975). The circular tunnel in elastic ground. *Geotechnique*. 25: 115–127.
- [18]. JSCE. (1996). Japanese standard for shield tunnelling. Tunnel Engineering Committee English Edition of Japanese Standard for Tunnelling, Subcommittee Japan Society of Civil Engineers. The third edition. Tokyo.
- [19]. Liu, J.H. and Hou, X.Y. (1991). Shield-driven tunnels. China Railway Press. Beijing. China. 152-303.
- [20]. Lee, K.M. and Ge, X.W. (2001). The equivalence of a jointed shield-driven tunnel lining to a continuous ring structure. *Canadian Geotechnical Journal*. 38: 461-483.
- [21]. Blom, C.B., Vander Horst, E.J. and Jovanovic, P.S. (1999). Three-dimensional structural analyses of the shield-driven “Green Heart” tunnel of the high-speed line south.
- [22]. Blom, C.B. (2002). Design philosophy of concrete linings for tunnel in soft soils. Ph.D. dissertation. Delft University. Netherlands.
- [23]. Nagggar, H.E. and Hinchberger, S.D. (2008). An analytical solution for jointed tunnel linings in elastic soil or rock. *Canadian Geotechnical Journal*. 45: 1572-1593.
- [24]. Kasper, T. and Meschke, G. (2004). A 3D finite element simulation model for TBM tunnelling in soft ground. *International Journal for Numerical and Analytical Methods in Geomechanics*. 28: 1441-1460.
- [25]. Kasper, T. and Meschke, G. (2006). A numerical study of the effect of soil and grout material properties and cover depth in shield tunnelling. *Computers and Geotechnics*. 33(4-5): 234-247.
- [26]. Hefny, A. and Chua, H. (2006). An investigation into the behavior of jointed tunnel lining. *Tunnelling and Underground Space Technology*. 21: 428.
- [27]. Munsterman, W.P. and Brugman, M.H.A. (2009). Determination of Final Geotechnical Parameters for Calculations. Mashhad Urban Railway Line 2. Rahab Engineering Establishment. Document No.: MUR2-ART-RE-01R04-01.
- [28]. ABAQUS software, analysis user’s guide, 2016.

## تأثیر درزه سگمنت بر روی نیروهای داخلی در پوشش تونل تحت بارگذاری لرزه ای به روش عددی

غلامحسین رنجبر<sup>1</sup>، کوروش شهريار<sup>2\*</sup> و کاوه آهنگری<sup>1</sup>

1- دانشکده فنی و مهندسی، واحد علوم و تحقیقات، دانشگاه آزاد اسلامی، تهران، ایران

2- دانشکده مهندسی معدن و متالورژی، دانشگاه صنعتی امیر کبیر، تهران، ایران

ارسال 2019/10/1، پذیرش 2020/4/23

\* نویسنده مسئول مکاتبات: k.shahriar@aut.ac.ir

### چکیده:

اگرچه پوشش سگمنتی تونل اغلب برای مناطق لرزه‌ای استفاده می‌شود، تأثیر درزه‌های سگمنت بر رفتار پوشش سگمنتی تحت بارگذاری لرزه‌ای در مطالعات پیشین کاملاً مورد توجه قرار نگرفته است. در این مقاله، نتایج یک مطالعه عددی بررسی تأثیر صلبیت چرخشی، محوری و شعاعی درزه‌های طولی بر روی نیروهای سازه در پوشش سگمنتی تونل تحت بارگذاری لرزه‌ای ارائه شده است. یک روش المان محدود سه بعدی برای ایجاد مدل‌های عددی از درزه‌ها استفاده شده است. اعتبار مدل عددی با مقایسه نتایج به دست آمده با روش‌های تحلیلی مشهور ارائه شده توسط وانگ و پنزین مورد آزمایش قرار گرفت. نتایج نشان می‌دهد که با افزایش صلبیت چرخشی درزه سگمنتی، ممان خمشی افزایش می‌یابد. زمانی که ضریب صلبیت چرخشی کمتر از  $0/5$  باشد، تغییرات ممان خمشی مثبت و منفی بیشتر است. نتایج مدل سازی عددی نشان می‌دهد تغییرات ممان خمشی و تفاوت بین مقادیر ممان خمشی مثبت و منفی با افزایش شتاب بارگذاری لرزه‌ای افزایش می‌یابد. علاوه بر این، برای مقادیر  $\lambda \geq 0/5$  قابل توجه است. با افزایش ضریب صلبیت چرخشی درزه سگمنتی، ضریب نیروی محوری کاهش می‌یابد. با افزایش ضریب صلبیت محوری و برشی درزه سگمنتی، تغییر ممان خمشی و نیروی محوری در پوشش سگمنتی جزئی است که می‌تواند برای طراحی پوشش سگمنتی نادیده گرفته شود.

**کلمات کلیدی:** پوشش سگمنتی، صلبیت درزه، بارگذاری لرزه‌ای، روش عددی، نیروهای داخلی.